Cyclotron masses and *g*-factors of hybridized electron-hole states in InAs/GaSb quantum wells

K. Nilsson,[1] A. Zakharova,[2] I. Lapushkin,[2] S. T. Yen,[3] and K. A. Chao[1]
[1]*Department of Physics, Lund University, Sölvegatan 14A, S223 62 Lund, Sweden*
[2]*Institute of Physics and Technology of the Russian Academy of Sciences, Nakhimovskii Avenue 34, Moscow 117218, Russia*
[3]*Department of Electronics Engineering, National Chiao Tung University, Hsinchu, Taiwan, Republic of China*
(Received 16 March 2006; revised manuscript received 21 June 2006; published 4 August 2006)

Using the eight-band $\mathbf{k}\cdot\mathbf{p}$ model and the Burt-Foreman envelope function theory to perform self-consistent calculations, we have studied the effect of electron-hole hybridization on the cyclotron masses m^* and the effective *g*-factors g^* of two-dimensional quasiparticles in InAs/GaSb quantum wells under a magnetic field applied perpendicular to the interfaces. We can modify the degree of hybridization by changing the InAs and/or GaSb layer width, or by inserting a thin AlSb barrier. While electron-light-hole hybridization dominates at both low and high fields, due to a sequence of anticrossings between electronlike and heavy-holelike levels, there is also an important contribution from heavy-hole states to the strong hybridization in the intermediate field range. The field-dependence of the hybridized energy eigenstates is manifested in the variations of m^* and g^*. Characteristic discontinuous changes of both m^* and g^* appear at each anticrossing, resulting in a magnetic-field-driven oscillating behavior of these quantities for electronlike states of a given Landau level index. The electron *g*-factor can change sign when two eigenstates anticross. Hybridization of electron and hole states enhances the electron effective mass, and we have found a complicated dependence of this effect on the interaction strength. Without inserting an AlSb barrier, the strong interaction between the electronlike and the light-holelike states at low magnetic fields produces a large level repulsion, and hence relatively small effective masses and *g*-factors associated with these states. Intermediate interaction leads to weaker level repulsion and therefore very heavy electron cyclotron masses as well as large *g*-factors associated with the lowest Landau levels. A weak interaction only enhances the cyclotron masses of the electronlike states slightly. The hole effective masses change with both the magnetic field and the sample structure in a more complicated fashion.

DOI: 10.1103/PhysRevB.74.075308 PACS number(s): 73.21.Ac, 73.21.Fg, 73.40.Kp

I. INTRODUCTION

Effective mass is a fundamental concept in semiconductor physics.[1] In bulk semiconductors the conduction band and the valence band are separated by an energy gap, and therefore the electron (hole) effective mass tensor elements are defined in terms of the energy band $E(\mathbf{k})$ as

$$\left[\frac{1}{m^*(\mathbf{k})}\right]_{ij} = \frac{1}{\hbar^2}\left|\frac{\partial^2 E(\mathbf{k})}{\partial k_i \partial k_j}\right|. \tag{1}$$

In this case, many dynamic properties of electrons (holes) in the conduction (valence) band can be conveniently described by the conduction (valence) band effective masses. This is also the situation in type-I semiconductor heterostructures where the conduction band of one semiconductor layer does not overlap with the valence band of any other semiconductor layer, and so an overall band gap exists. However, in type-II semiconductor heterostructures such as InAs/GaSb, which is commonly referred to as a broken-gap heterostructure, the conduction band of one semiconductor layer overlaps with the valence band of another semiconductor layer. In the vicinity of the band-overlap region, conduction band states hybridize with valence band states. How to define the effective masses of the hybridized eigenstates and use them to describe the dynamic properties of the corresponding quasiparticles is an interesting and important problem.

InAs/GaSb based broken-gap heterostructures, such as InAs/Al_xGa_{1-x}Sb quantum wells and InAs/GaSb superlattices, have been investigated experimentally with cyclotron resonance and optical measurements,[2–8] as well as with transport (including magnetotransport) studies.[9–15] Transport data[13,14] revealed the existence of the theoretically predicted[16] hybridization gaps in the two-dimensional (2D) carrier dispersions.[13,14] The origin of these hybridization gaps is the anticrossings of the 2D electron and hole subbands. Cyclotron resonance experiments[5–8,15] were performed to measure the electron effective mass, which was found larger than its corresponding bulk value. This enhancement of the effective mass was explained with the hybridization of electron and heavy-hole states.[17,18] The experimental effective mass varies when the InAs layer thickness is changed or when spacer layers are added.[5,8] It was also reported that the effective mass oscillates with the magnetic field.[6,7] The observed splitting of the cyclotron resonance peak is a consequence of different Zeeman splittings of closely separated Landau levels.[5,7,8,15]

Most theoretical works on the hybridization of electron and hole levels have restricted themselves to the situation without an applied magnetic field.[16,19–22] Existing theoretical investigations of this problem in the presence of an applied magnetic field mainly considered hybridization of electrons and heavy holes and its effect on Landau level structures, cyclotron masses, and *g*-factors.[17,18,23] These studies found anticrossings and energy gaps in the Landau level structure resulting from the hybridization. The discovered oscillations of the heavy-hole *g*-factors with the magnetic field were caused by the Landau level index changes at the anticrossings[23] whereas the electron effective mass oscillations were caused by changing filling factors.[17,18] In addition,

electrons can also hybridize strongly with light holes,[21] and possibly hybridize simultaneously with both heavy holes and light holes.[22] Such a hybridization should also influence the electron and hole effective masses and g-factors. Clearly, the cyclotron masses and g-factors of quasiparticles in broken-gap heterostructures require further investigations.

In this paper we use the Burt-Foreman envelope function theory[24,25] to investigate the influence of the hybridization of electron, light-hole, and heavy-hole states on Landau level structures, electron and hole cyclotron masses, and effective g-factors in AlSb/InAs/GaSb/AlSb quantum wells under a magnetic field applied perpendicular to the interfaces. In contrast to the previous non-self-consistent six-band calculations of electron cyclotron masses[18] and g-factors,[23] we will here include the effect of charge transfer and use the eight-band $\mathbf{k}\cdot\mathbf{p}$ model. The carrier transfer through the InAs/GaSb interfaces significantly modifies the band-edge positions and the dispersions in InAs/GaSb superlattices[16] and quantum wells.[26] This effect is much more important than the inclusion of the split-off band and is needed to derive accurate results. Additionally we take the effects of the lattice-mismatch induced strain into account, which also modifies the Landau level structures in InAs/GaSb quantum wells.[23]

In Sec. II we describe the model Hamiltonian, which is an extended version of the Hamiltonian in Ref. 23, and the basis expansion method for solving the Schrödinger equation. With this efficient new method of calculation, which was rarely used before, one can show clearly that the Hamiltonian matrix is real and symmetric. The energy level structure will be presented in Sec. III, where the degree of electron-hole hybridization is found to be sensitive to the geometric structure of the sample and the magnetic field strength. These results are used in Sec. IV to understand the unusually interesting features obtained for the cyclotron masses and effective g-factors. In particular the cyclotron masses of the electronlike and of the light-holelike states have a nonmonotonic dependence on the interaction strength. For the lowest electronlike eigenstate, the cyclotron mass and the effective g-factor exhibit oscillating behavior within a certain range of the magnetic field strength. For the hybridized heavy-holelike states unusually large effective g-factors are found. The results for the cyclotron masses are entirely new, whereas the behavior of the g-factors under a magnetic field is quite different from that derived in Ref. 23 with a non-self-consistent six-band calculation. The origin of this difference is explored in Sec. V, and is found to be the self-consistent potential. The effect of the self-consistent potential on the effective mass is also investigated. There are recent experiments on broken-gap heterostructures, and a comparison between our calculations and the measured data is discussed in Sec. VI. In the final Sec. VII we will give a conclusion. Because the matrix elements of the eight-band $\mathbf{k}\cdot\mathbf{p}$ model Hamiltonian are very complicated, to be self-content, their explicit expressions are listed in the Appendix.

II. HAMILTONIAN AND EIGENSOLUTIONS

The system under study is an InAs/GaSb broken-gap quantum well sandwiched between two AlSb barriers. The self-consistently calculated band-edge profile is shown in Fig. 1, where also the coordinate system and the crystal axes are specified. The sample is grown along the [001] direction on a GaSb substrate, meaning that the InAs layer is strained. An external magnetic field B is applied perpendicular to the interfaces.

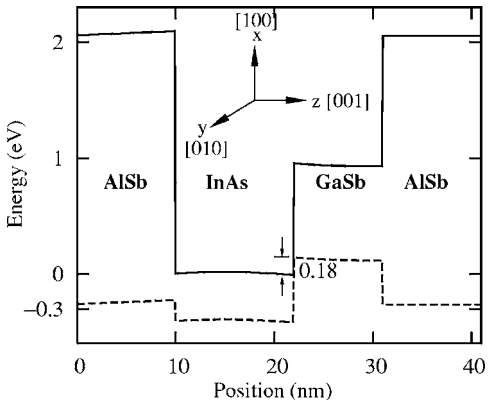

FIG. 1. The self-consistently calculated band diagram of the AlSb/InAs/GaSb/AlSb structure with a 12 nm InAs and a 9 nm GaSb layer.

In the absence of a magnetic field, we write the eight-band $\mathbf{k}\cdot\mathbf{p}$ Burt-Foreman Hamiltonian[27] at the Γ point in a zinc-blende crystal as $\hat{H}_8'=\hat{H}_k+\hat{H}_\varepsilon$, where $\hat{H}_k$ includes the $\mathbf{k}$-dependent part and the spin-orbit interaction, and $\hat{H}_\varepsilon$ represents the effect of strain on the energy levels. When an external magnetic field B is applied in the z-direction, we use the Landau gauge $(A_x,A_y,A_z)=(0,Bx,0)$ and replace the kinetic momentum operators $\hat{k}_i$ in $\hat{H}_k$ by the canonical momentum operators $\hat{K}_i=\hat{k}_i+eA_i/\hbar$, where $e>0$ is the elementary charge. Starting from the explicit form of the Hamiltonian which is given in Ref. 27, we apply the unitary transformation outlined in Ref. 28 to the set of basis functions $\{|s_{1/2,1/2}\rangle,|p_{3/2,1/2}\rangle,|p_{1/2,1/2}\rangle,|p_{3/2,3/2}\rangle,|s_{1/2,-1/2}\rangle,|p_{3/2,-1/2}\rangle,|p_{1/2,-1/2}\rangle,|p_{3/2,-3/2}\rangle\}$. For convenience we change the phase of the last basis function by a minus sign. Adding the Zeeman interaction term $\hat{H}_Z$ our model Hamiltonian is expressed as

$$\hat{H}_8=\begin{pmatrix}\hat{H}_{-+} & \hat{H}_{--}\\ \hat{H}_{++} & \hat{H}_{+-}\end{pmatrix}+\begin{pmatrix}\hat{H}_{\varepsilon,4} & 0\\ 0 & \hat{H}_{\varepsilon,4}\end{pmatrix}+\begin{pmatrix}\hat{H}_{Z,4} & 0\\ 0 & -\hat{H}_{Z,4}\end{pmatrix}. \tag{2}$$

To explicitly write down the $\mathbf{k}$-dependent parts $\hat{H}_{\pm\mp}$ and $\hat{H}_{\pm\pm}$, let us define $E_c(z)$ and $E_v(z)$ as the conduction and valence band edges, $\Delta(z)$ as the split-off energy, $A_c(z)$ as a parameter which describes the effect of remote bands on the electron effective mass, and $P(z)$ as the interband momentum matrix element. In terms of $\hat{K}_\pm=\mp i(\hat{K}_x\pm i\hat{K}_y)/\sqrt{2}$ and the operators which are defined in the Appendix, we have

$$\hat{H}_{\pm\mp} = \begin{pmatrix} E_c + \hat{A} & \sqrt{2}iP\hat{K}_z/\sqrt{3} & -iP\hat{K}_z/\sqrt{3} & \pm P\hat{K}_\pm \\ -\sqrt{2}i\hat{K}_z P/\sqrt{3} & E_v + \hat{G}_\pm & \hat{D}_\pm & \pm\hat{S}_\pm \\ i\hat{K}_z P/\sqrt{3} & \hat{D}_\pm & E_v - \Delta + \hat{E}_\pm & \mp\hat{S}_\pm/\sqrt{2} \\ \pm\hat{K}_\mp P & \pm\hat{S}_\pm^\dagger & \mp\hat{S}_\pm^\dagger/\sqrt{2} & E_v + \hat{F}_\pm \end{pmatrix} \tag{3}$$

and

$$\hat{H}_{\pm\pm} = \begin{pmatrix} 0 & P\hat{K}_\pm/\sqrt{3} & \sqrt{2}P\hat{K}_\pm/\sqrt{3} & 0 \\ \hat{K}_\pm P/\sqrt{3} & \hat{T}_\pm & \hat{P}_\pm & \pm\hat{R}_\pm \\ \sqrt{2}\hat{K}_\pm P/\sqrt{3} & \hat{Q}_\pm & -\hat{T}_\pm & \pm\sqrt{2}\hat{R}_\pm \\ 0 & \mp\hat{R}_\pm & \mp\sqrt{2}\hat{R}_\pm & 0 \end{pmatrix}. \tag{4}$$

The fourth Luttinger parameter κ does not appear explicitly in the above matrix elements because we have already rewritten κ in terms of three other Luttinger parameters γ_1, γ_2, and γ_3. This is explained in more detail in the Appendix.

The strain part $\hat{H}_{\varepsilon,4}$ of the Hamiltonian has the matrix representation

$$\hat{H}_{\varepsilon,4} = \begin{pmatrix} a_c\varepsilon & 0 & 0 & 0 \\ 0 & S_1 & S_2 & 0 \\ 0 & S_2 & S_3 & 0 \\ 0 & 0 & 0 & S_4 \end{pmatrix} \tag{5}$$

with matrix elements

$$S_1 = \left(a_v - \frac{b}{2}\right)2\varepsilon_{xx} + (a_v + b)\varepsilon_{zz}, \tag{6a}$$

$$S_2 = \sqrt{2}b(\varepsilon_{xx} - \varepsilon_{zz}), \tag{6b}$$

$$S_3 = a_v(2\varepsilon_{xx} + \varepsilon_{zz}), \tag{6c}$$

$$S_4 = \left(a_v + \frac{b}{2}\right)2\varepsilon_{xx} + (a_v - b)\varepsilon_{zz}. \tag{6d}$$

In the above expressions $a_c(z)$ is the conduction band deformation potential, and $a_v(z)$ and $b(z)$ are the valence band deformation potentials. Because our structure is grown along the [001] crystal axis, which we define as the z axis, the only nonvanishing strain tensor components are ε_{zz} and $\varepsilon_{xx}=\varepsilon_{yy}$, which are defined in Ref. 23.

Finally, the Zeeman interaction term $\hat{H}_{Z,4}$ has the simple matrix representation

$$\hat{H}_{Z,4} = \mu_B B \begin{pmatrix} 1 & 0 & 0 & 0 \\ 0 & 1/3 & -2\sqrt{2}/3 & 0 \\ 0 & -2\sqrt{2}/3 & -1/3 & 0 \\ 0 & 0 & 0 & 1 \end{pmatrix}, \tag{7}$$

where μ_B is the Bohr magneton.

We would like to list the terms which are neglected in our model Hamiltonian and explain the reason for doing so. First, we have ignored the terms linear in k in the valence band Hamiltonian, and the terms proportional to Kane's B-parameter. The effect of these terms is to produce a spin split of the Landau levels, which is negligibly small as compared to those produced by the Zeeman and Rashba effects. Second, we have neglected the spin-orbit interaction terms in the strain Hamiltonian. Although these terms can contribute to the spin split of the levels in the valence band quantum well,[29] in our samples the GaSb layer is unstrained and therefore these terms do not influence the energy level positions of the hybridized electron-hole states. Also, we neglect the parameters q and N_1 defined in Ref. 30, because they are small.

The Hamiltonian Eq. (2) based on the Burt-Foreman envelope function theory[24,25] is Hermitian, although its matrix elements may not be Hermitian. We solve the Schrödinger equation

$$\hat{H}_8\Psi = E\Psi \tag{8}$$

self-consistently with the Poisson equation[26] to obtain the band-edge profile E_c and E_v, as well as the eigenenergies E and envelope functions Ψ. It is important to point out that the self-consistent correction to the potential profile in unbiased samples, which is the case considered in this paper, is much less than the change of potential profile caused by an externally applied electric field. For the samples studied in this paper, where the layers are thin and the magnetic fields smaller than 17 T, the self-consistent correction is insensitive to the applied magnetic field strength. Therefore it is justified to simplify the problem and use the zero-magnetic-field self-consistent potential throughout the entire calculation. Nevertheless, as we will show later in our numerical results, the effect of charge transfer is important to derive accurate Landau level structures, and consequently it modifies the cyclotron effective mass and effective g-factor.

To solve the Schrödinger equation we use a basis expansion method.[31] Because of the confinement imposed by the quantum well it is most convenient to use a set of basis functions which are localized within the quantum well. Hence we choose $\{\phi_\mu(z)=\sqrt{2/L}\sin(\mu\pi z/L);\ \mu=1,2,\ldots,N\}$ as our basis functions, where L is the length of the sample in the z-direction. In principle N should be infinite. However, in our numerical calculation we set N as a large finite number.

The envelope function Ψ is a vector function with eight components Ψ_j for $j=1,2,\ldots,8$. We transform Eq. (8) into a matrix equation using the expansion

$$\Psi_j = \exp(ik_y y) F_{\nu_j}(x') \sum_{\mu=1}^{N} \phi_\mu(z) C_{\mu j}, \tag{9}$$

where $F_\nu(x')$ are the normalized harmonic oscillator functions with $x'=x+k_y/s$ and $s=eB/\hbar$. Let us define a column vector $\mathbf{C}$ with $8N$ components $C_{(j-1)N+\mu} \equiv C_{\mu j}$ with $j=1,2,\ldots,8$ and $\mu=1,2,\ldots,N$. Then Eq. (8) becomes

$$\mathcal{H}\mathbf{C} = E\mathbf{C}. \tag{10}$$

We should pay attention to the relationship[32] between j and the Landau level quantum number ν_j. In terms of an integer n, the values of ν_j are $\nu_1=\nu_2=\nu_3=n$, $\nu_4=n-1$, $\nu_5=\nu_6=\nu_7=n+1$, and $\nu_8=n+2$. Since $\nu_j \geqslant 0$, we must set $n \geqslant -2$. The size of the matrix $\mathcal{H}$ depends on both n and the number of basis functions N.

In the above expansion we have used the axial approximation to neglect the warping terms in the $\hat{R}_\pm$ operators, which are proportional to $(\gamma_2-\gamma_3)$. This approximation allows us to express Ψ_j as a finite sum of N basis functions as given in Eq. (9). In other words, $\mathcal{H}$ can be diagonalized for each n separately. To justify the validity of the axial approximation, we have summed over the quantum numbers ν_j in Eq. (9) and found that the Landau level structure is insensitive to this procedure.

The matrix elements

$$\mathcal{H}_{\mu j,\eta i} = \langle \exp(-ik_y y) F_{\nu_j} \phi_\mu | (\hat{H}_8)_{ji} | \exp(ik_y y) F_{\nu_i} \phi_\eta \rangle \tag{11}$$

are evaluated analytically. With our choice of basis functions their final analytical form clearly shows that the Hamiltonian matrix is real and symmetric, and therefore Hermitian. Because our sample has layer structure, all material parameters in the Hamiltonian are piecewise-constant functions of z. Let us consider $Q(z)$ as an example. In the mth layer of the heterostructure ($z_m \leqslant z < z_{m+1}$), $Q(z)$ is a constant Q_m. To perform the analytical work, $Q(z)$ is expressed in terms of the Heaviside step function $\Theta(z)$ as

$$Q(z) = \sum_{m=0}^{M-1} (Q_m - Q_{m-1}) \Theta(z - z_m). \tag{12}$$

In our notation we set $z_0=0$, $z_M=L$, and $Q_{-1}=0$.

With the basis expansion method, through the eigenvectors $\mathbf{C}$, we can easily classify the levels. For an eigenenergy E_i, we define[33]

$$d_I(B) = \sum_{\mu, j \in I} |C_{\mu j}(E_i, B)|^2 \tag{13}$$

as the relative contribution to this level from the basis states in the set I. $d_I(B)$ is so normalized that if we include all states in the set I, then $d_I(B)=1$. In the present work, we will calculate d_e for the contribution from the $|s_{1/2,\pm 1/2}\rangle$ states, d_{lh} for the contribution from the $|p_{3/2,\pm 1/2}\rangle$ states, and d_{hh} for the contribution from the $|p_{3/2,\pm 3/2}\rangle$ states. For example, to calculate d_e from Eq. (13), we let I contain $j=1,5$ and $\mu=1,2,\ldots,N$. In a similar way we can calculate the contribution from states with a specific Landau level quantum number ν.

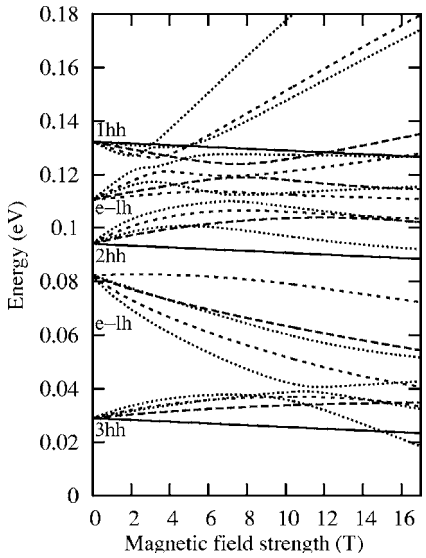

FIG. 2. Eigenenergy level structure for an InAs/GaSb quantum well with a 12 nm InAs layer and a 9 nm GaSb layer. Solid curves are for the levels with $n=-2$, long-dashed curves for $n=-1$, short-dashed curves for $n=0$, and dotted curves for $n=1$.

To close this section, we should mention that the difference between our model and that in Ref. 34 is that here we have included the split-off band. Also, the Zeeman interaction is included in our model Hamiltonian but not in the one treated in Ref. 30. In fact, the Zeeman interaction effects the heavy-hole g-factors significantly.

III. HYBRIDIZATION EFFECTS ON ENERGY LEVEL STRUCTURES

To investigate the effects of hybridization on the energy levels and later on the effective masses and g-factors in broken-gap quantum wells, we will study two types of samples. The first one is the AlSb/InAs/GaSb/AlSb structure as shown in Fig. 1. Here we will vary the thicknesses of both the InAs layer and the GaSb layer, which determine the positions of the quantum confined energy levels. We then create the second sample type by inserting a thin AlSb barrier between the InAs and GaSb layers. In this way the overlap of the conduction band states and the valence band states can be controlled directly. In our numerical calculations we take the material parameters from Refs. 21 and 35, and use 100 basis functions. We will first study hybridization between electronlike states and light-holelike states, which exists already in the absence of an external magnetic field. Under a finite magnetic field hybridization with heavy-holelike states will emerge. Numerical results will be shown in Figs. 2–5. In all these figures, solid curves are for energy levels with $n=-2$, long-dashed curves are for $n=-1$, short-dashed curves are for $n=0$, and dotted curves are for $n=1$.

Most studies of the Landau level structures of quasiparticles in semiconductor heterostructures have used the six-band $\mathbf{k}\cdot\mathbf{p}$ model, while few works are based on the eight-band $\mathbf{k}\cdot\mathbf{p}$ model. One finds only a slight quantitative difference in the energy level structure near the Fermi energy

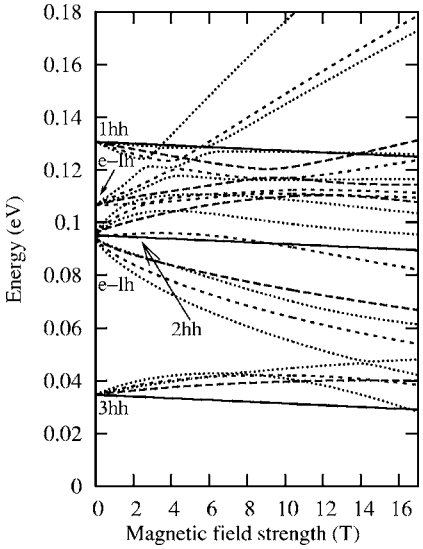

FIG. 3. Similar eigenenergy level structure as in Fig. 2, but the sample has a 1 nm AlSb barrier inserted between the InAs layer and the GaSb layer in the quantum well.

between the six-band and the eight-band results. When carriers appear in doped structures, the self-consistent correction to the potential profile becomes very important as mentioned in the previous section. We will return to this point later after we have presented our self-consistent numerical results on the energy level structures, the cyclotron effective mass, and the effective g-factor.

We start with a typical quantum well as shown in Fig. 1 with a 12 nm thick InAs layer and a 9 nm GaSb layer, and calculate the energy levels under magnetic fields up to $B=17$ T. The energy levels within the quantum well are plotted in Fig. 2. These levels are labeled according to their primary characters at zero magnetic field: e for electronlike, lh for light-holelike, and hh for heavy-holelike. In the absence of the magnetic field $B=0$, electron states and light-

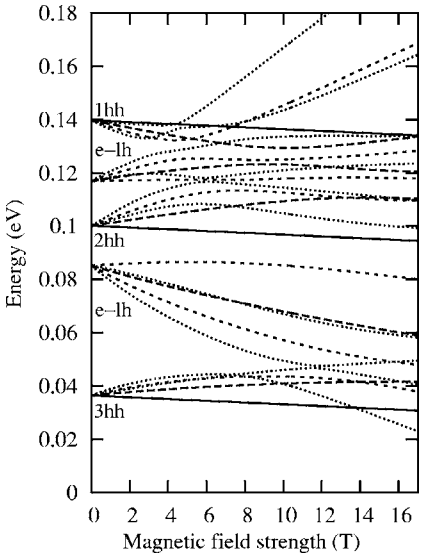

FIG. 4. Similar eigenenergy level structure as in Fig. 2, but with a 9 nm InAs layer and a 9 nm GaSb layer.

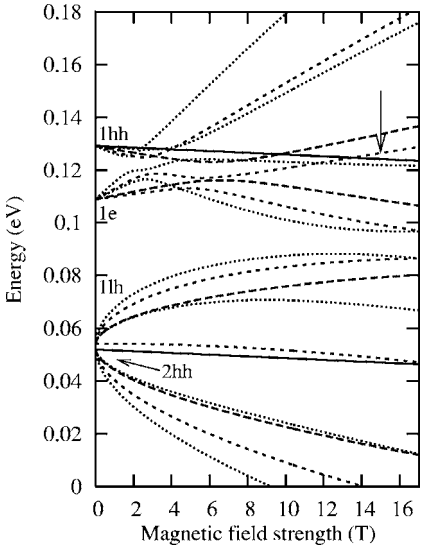

FIG. 5. Similar eigenenergy level structure as in Fig. 2, but with a 12 nm InAs layer and a 6 nm GaSb layer.

hole states already mix, and the two hybridized levels are marked as e-lh. Let us define $\Delta_{e\text{-}lh}$ as the energy separation between these two hybridized levels at $B=0$. In Fig. 2 $\Delta_{e\text{-}lh}$ is about 30 meV. Using Eq. (13) we have calculated the relative contributions d_e from the $|s_{1/2,\pm 1/2}\rangle$ states and d_{lh} from the $|p_{3/2,\pm 1/2}\rangle$ states. We found $d_e(B=0)=0.56$ and $d_{lh}(B=0)=0.44$ for the upper e-lh level, and $d_e(B=0)=0.34$ and $d_{lh}(B=0)=0.66$ for the lower e-lh level. These values of $\Delta_{e\text{-}lh}$, d_e, and d_{lh} indicate a strong e-lh hybridization. The level structure becomes complicated with increasing magnetic field strength, and we will return to this aspect later after we have fully analyzed the situation at zero magnetic field.

To control the degree of hybridization, we can change the sample structure by inserting a barrier or varying the widths of the InAs layer and the GaAs layer. First we consider the barrier effect. Between the 12 nm InAs layer and the 9 nm GaSb layer we insert a 1 nm AlSb barrier which reduces the overlap between the wave functions in the InAs layer and those in the GaSb layer. There exists experimental studies[7] on this type of samples, and we will check the experimental data later. Because we retain the layer width of both InAs and GaSb when inserting the AlSb barrier, the effect of the barrier on the heavy-holelike levels is insignificant. However, the energy separation $\Delta_{e\text{-}lh}$ is drastically reduced by the AlSb barrier. Our calculated level structure, shown in Fig. 3, exhibits a $\Delta_{e\text{-}lh} \simeq 10$ meV. This is much less than the corresponding $\Delta_{e\text{-}lh} \simeq 30$ meV in Fig. 2. Hence in the absence of the 1 nm AlSb barrier, the two e-lh states repel each other. The origin of this strong repulsion is the strong interaction of the two levels in Fig. 3 which are very close to each other. The calculated values of $d_l(B)$ are $d_e(B=0)=0.33$ and $d_{lh}(B=0)=0.67$ for the upper e-lh level, and $d_e(B=0)=0.57$ and $d_{lh}(B=0)=0.43$ for the lower one. Consequently, the main effect of the inserted barrier is on $\Delta_{e\text{-}lh}$ but not on $d_e(B=0)$ and $d_{lh}(B=0)$. In addition, inserting the barrier results in an anticrossing of the two e-lh states.

Next we examine the effect of layer thickness on the hybridization. Let us return to Fig. 1 and study a quantum well

with a 9 nm InAs layer and a 9 nm GaSb layer. This change of layer width slightly alters all energy level positions, which can be seen by comparing our calculated levels in Fig. 4 with those plotted in Fig. 2. It is important to notice that the energy separation $\Delta_{e\text{-}lh} \simeq 34$ meV in Fig. 4 is larger than the corresponding 30 meV in Fig. 2. This increase of $\Delta_{e\text{-}lh}$ is due to the slight upward-shift of the electronlike level when the InAs layer width is reduced from 12 to 9 nm. However, the hybridization between the electronlike and the light-holelike states is still fairly strong. The relative contributions are $d_e(B=0)=0.36$ and $d_{lh}(B=0)=0.64$ for the upper *e-lh* level, and $d_e(B=0)=0.43$ and $d_{lh}(B=0)=0.55$ for the lower *e-lh* level. These numbers do not suggest the existence of two light-holelike levels because the nonparabolicity of the InAs conduction band and the narrow band gap produce a significant contribution of the $|p_{3/2,\pm 1/2}\rangle$ states to the electron wave function. The highest *e-lh* state changes its character from light-holelike at $B=0$ to electronlike at finite magnetic fields. For the electronlike state at $B=0$, d_{lh} is larger than the d_{lh} of the corresponding state in the structure with a thicker InAs layer. Hence the hybridization of the two *e-lh* states is stronger in the structure with a 9 nm InAs layer. If we insert a 1 nm AlSb barrier in the well and repeat the calculation, we obtain $d_e(B=0)=0.70$ and $d_{lh}(B=0)=0.27$ for the upper *e-lh* level, and $d_e(B=0)=0.14$ and $d_{lh}(B=0)=0.82$ for the lower *e-lh* level, indicating a significant reduction of the hybridization. When the 1 nm AlSb barrier is removed, due to the reducing interaction strength, the repulsion of two *e-lh* levels becomes weaker than that in the structure with a 12 nm InAs layer and a 9 nm GaSb layer.

Finally we reduce the GaSb layer thickness and calculate the energy levels in a quantum well with a 12 nm InAs layer and a 6 nm GaSb layer. This will lower the hole levels and so weaken the mixing of the electron and light-hole states. Figure 5 shows the result in which the hybridization of the electronlike and the light-holelike states is much less than those in the other structures. The interaction between these levels is also very small. This can be easily checked by the fact that inserting a 1 nm AlSb barrier in the well produces only slight changes of the *e-lh* level positions at $B=0$.

After thoroughly analyzing the zero-magnetic-field case, we now examine the magnetic effect on the level hybridization. In all four figures 2–5 the anticrossings with heavy-holelike states emerge first with the 1*hh*-levels, then with the 2*hh*-levels, and finally with the 3*hh*-levels. For each eigenenergy the behavior of hybridization can only be analyzed numerically by calculating $d_e(B)$, $d_{lh}(B)$, and $d_{hh}(B)$. As an illustrating example we will perform such an analysis on the $n=0$ electronlike eigenstate in Fig. 5, whose eigenenergy is indicated by the downward arrow. At low magnetic fields, below ~2 T, and at high magnetic fields, above ~8 T, both electronlike states and heavy-holelike states hybridize mainly with the light-holelike states. In the region of magnetic field between 2 and 8 T we find an interesting and complicated hybridization behavior involving all three types of states. The eigenenergy of the $n=0$ electronlike eigenstate is replotted in Fig. 6 as the short-dashed curve using the vertical scale at the right-hand side. Along with this eigenenergy, the calculated relative contributions are plotted with the

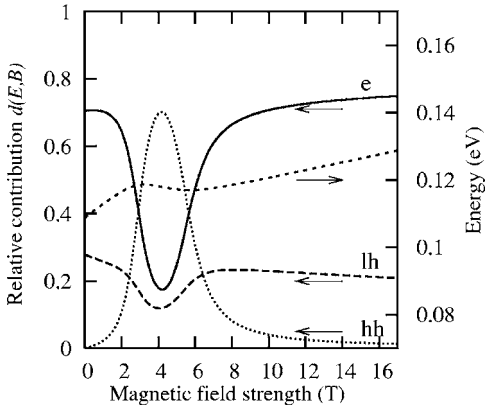

FIG. 6. Relative contributions from the $|s_{1/2,\pm 1/2}\rangle$, the $|p_{3/2,\pm 1/2}\rangle$, and the $|p_{3/2\pm 3/2}\rangle$ states to the $n=0$ eigenenergy level which is indicated by the arrow in Fig. 5.

solid curve for $d_e(B)$, the long-dashed curve for $d_{lh}(B)$, and the dotted curve for $d_{hh}(B)$. At low magnetic fields this eigenstate is mainly electronlike with $\nu=1$ and spin down. As the field increases to around $B=2$ T it anticrosses with the $n=0$ state in the 1*hh* level and becomes heavy-holelike with $\nu=2$ and spin down. The second anticrossing occurs around $B=6$ T and is with another electronlike $n=0$ state. After this anticrossing the eigenstate becomes electronlike again but with $\nu=0$ and spin up. We also see in Fig. 6 a fair amount of contributions from light-hole states at all field strengths. Especially in the region from 2 to 7 T, all electron, light-hole and heavy-hole states mix simultaneously as indicated in Fig. 6. The energy separation between the two *e-lh* levels increases with the field, and the higher *e-lh* level becomes increasingly electronlike while the lower one becomes light-holelike. We found similar behavior for other sample structures. The hybridization of various states significantly affects the cyclotron effective mass and *g*-factor as is discussed below.

IV. EFFECTIVE MASS AND *g*-FACTORS

In the independent-particle model the cyclotron effective mass m^* is defined as $m^*=eB/\omega_c$, where ω_c is the cyclotron frequency. Because the energy separation $\delta\epsilon(\nu,\sigma)$ between the (ν,σ) Landau level and $(\nu+1,\sigma)$ Landau level is a constant with value $\hbar\omega_c$ for all values of ν and spin σ, the effective mass of a noninteracting particle is independent of its eigenenergy as is easily seen if we rewrite the effective mass as $m^*(\nu,\sigma)=\hbar eB/\delta\epsilon(\nu,\sigma)$. The same conclusion applies to the effective *g*-factor which is defined as $g^*=\delta\epsilon_{\uparrow\downarrow}(\nu)/\mu_B B$, where $\delta\epsilon_{\uparrow\downarrow}(\nu)$ is the energy separation between eigenstates with opposite spins but the same ν. The situation is quite different in broken-gap heterostructures in which the degree of hybridization between electron, light-hole, and heavy-hole states is sensitive to the strength of the applied magnetic field. Consequently, both m^* and g^* depend on the spin-orbital eigenstates of two adjacent eigenenergies. This dependence can cause a sign change of g^* because of the energy level anticrossings. The problem can only be explored with a numerical approach and here we will study the

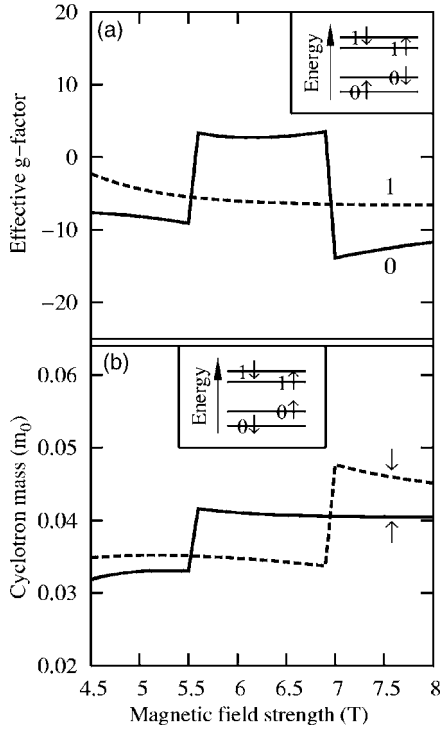

FIG. 7. Effective g-factors $g^*_{e,0}$ and $g^*_{e,1}$ for the electronlike states in Fig. 5 [panel (a)], and the corresponding cyclotron masses $m^*_{e,\uparrow}$ and $m^*_{e,\downarrow}$ [panel (b)]. The inset in panel (a) shows the relative positions (not to scale) of the eigenenergy levels above the magnetic field 7 T, and the one in panel (b) is for the relative positions of the eigenenergy levels in the range of magnetic field between 5.5 and 7 T.

characteristic features of m^* and g^*, using four spin-orbital eigenstates as an illustrative example. These eigenstates have $\nu=0$ or $\nu=1$ and will be labeled as $0\uparrow$, $0\downarrow$, $1\uparrow$, and $1\downarrow$.

Based on the results in Figs. 5 and 6 in the previous section we have studied the hybridization phenomena in detail in the quantum well with a 12 nm InAs layer and a 6 nm GaSb layer. At low and high magnetic fields both electronlike states and heavy-holelike states mainly hybridize with light-holelike states. The most interesting magnetic field region is around 4 T where all three types of states mix together. Therefore it is most informative to analyze the behavior of m^* and g^* around this magnetic field strength, and we will do it first. The calculated results for the electronlike level are given in Fig. 7 with panel (a) for the effective g-factor and panel (b) for the effective mass in units of the free electron mass m_0. In panel (a) the solid curve is associated with the $0\uparrow$ and $0\downarrow$ states, while the dashed curve is associated with the $1\uparrow$ and $1\downarrow$ states. Similarly, in panel (b) the solid curve is for the $\uparrow$-states ($0\uparrow$ and $1\uparrow$), and the dashed curve is for the $\downarrow$-states ($0\downarrow$ and $1\downarrow$).

We see many anticrossings if we follow the electronlike energy level in Fig. 5. When an anticrossing occurs the values of the corresponding m^* and g^* change abruptly. We notice that in Fig. 6 the solid curve and the dotted curve cross each other twice at two values of magnetic field below and above 4 T. To clarify the phenomenon of the sudden changes of m^* and g^*, it is sufficient to consider the region of magnetic field $B>4$ T, where two anticrossings appear around 5.5 and 7 T. Let us examine what happens around $B=7$ T. In the region between 5.5 and 7 T, the relative positions of the relevant energy levels are shown by the insert in panel (b). The $0\uparrow$ (or $1\downarrow$) level is higher than the $0\downarrow$ (or $1\uparrow$) level. Therefore in panel (a) the solid curve is positive while the dashed curve is negative. On the other hand, the energy separation between the two $\uparrow$-spin states $0\uparrow$ and $1\uparrow$ is smaller than that between the two $\downarrow$-spin states $0\downarrow$ and $1\downarrow$. The $\uparrow$-spin effective mass is then larger than the $\downarrow$-spin effective mass, as indicated in panel (b). At the anticrossing around $B=7$ T, the $0\downarrow$ level moves to a position above the $0\uparrow$ level such that the $0\downarrow$-$1\downarrow$ level separation becomes smaller than the $1\uparrow$-$0\uparrow$ level separation. The resulting relative energy level positions are plotted in the insert in panel (a). Consequently, the g^* associated to the $0\downarrow$-$0\uparrow$ levels becomes negative, and the $\downarrow$-spin effective mass becomes heavier than the $\uparrow$-spin effective mass.

The electron effective mass in bulk InAs is $0.024m_0$, where m_0 is the free electron mass. Our calculated results given in Fig. 7 indicate a strong enhancement of the effective mass of electronlike quasiparticles, which has been observed experimentally.[6–8] The origin of this enhancement lies in the fact that each electronlike wave function has components of electron parts from the InAs layer and hole parts from the GaSb layer, and the hole effective mass is larger than the electron effective mass. This also explains the sudden change of the electronlike effective mass when its hybridization with the heavy-holelike states occurs. Consequently, if the changing magnetic field strength can induce a series of anticrossings involving the electronlike and the heavy-holelike states, we expect to see oscillations of the effective mass with the applied field. Whether such oscillation can be observed in experiments depends on the position of Fermi energy. It is worthwhile to mention that oscillations of the effective mass have been observed experimentally[6] by changing the filling of Landau levels with the applied magnetic field. We should also point out that our discovered cyclotron mass oscillations for electronlike states occur with fixed Landau level indices, whereas the mass oscillations obtained in the previous investigation[18] appear with changing Landau level indices.

Because the effective mass m^* and the effective g-factor g^* in broken-gap heterostructures are sensitive to hybridization, which varies with the sample structure and with the applied magnetic field strength, it is impossible to predict their features analytically. Here we provide some general information for three typical quantum well structures in terms of the layer widths, and at three values of magnetic field. Table I shows effective masses for the highest $1e$-$1lh$ states and $1hh$-like states, $m^*_{e,\sigma}$ and $m^*_{hh,\sigma}$, and Table II shows the effective g-factors $g^*_{e,\nu}$ and $g^*_{hh,\nu}$. We see clearly in Table I that in all cases the electronlike effective masses are enhanced over the value $0.024m_0$ in bulk InAs. At low magnetic fields, the interaction between the two hybridized e-lh levels in the 12 nm InAs and 9 nm GaSb structure is stronger than that in the 9 nm InAs and 9 nm GaSb structure, leading to smaller effective masses in the structure with a 12 nm InAs layer. Similarly, the electron mass enhancement is very small in the quantum well with the 6 nm GaSb layer, there

TABLE I. Effective masses for the highest electron-like states ($m^*_{e,\sigma}$) and for the highest heavy-hole-like states ($m^*_{hh,\sigma}$) in a quantum well with InAs layer width W_{InAs} and GaSb layer width W_{GaSb}, calculated from the energy difference between the 0σ and the 1σ states for $\sigma=\uparrow$ and $\downarrow$.

(W_{InAs}; W_{GaSb})	B (T)	$m^*_{e,\uparrow}$	$m^*_{e,\downarrow}$	$m^*_{hh,\uparrow}$	$m^*_{hh,\downarrow}$
(12 nm; 9nm)	1	0.05534	0.05523	0.1175	0.1019
(12 nm; 9nm)	10	0.04363	0.04526	0.3491	0.1058
(12 nm; 9nm)	15	0.04247	0.04398	0.3974	0.07226
(9 nm; 9nm)	1	0.09599	0.08885	0.1193	0.1051
(9 nm; 9nm)	10	0.06273	0.05229	0.4241	0.1654
(9 nm; 9nm)	15	0.05600	0.05770	0.3988	0.07259
(12 nm; 6nm)	1	0.04687	0.04477	0.1340	0.1145
(12 nm; 6nm)	10	0.04062	0.04350	0.2174	0.09710
(12 nm; 6 nm)	15	0.04131	0.04345	0.2851	0.1111

this interaction is even weaker. The electron-light-hole hybridization is reduced with increasing magnetic field, and consequently the electron cyclotron masses are smaller at high magnetic fields, especially for the structures with a 9 nm GaSb layer.

On the other hand, comparing with the heavy-hole effective mass $0.34m_0$ in bulk GaSb, the values of $m^*_{hh,\uparrow}$ and $m^*_{hh,\downarrow}$ listed in Table I can be either enhanced or suppressed, depending on the sample structure and the magnetic field strength, which determine the details of hybridization and anticrossing. For all samples at low magnetic fields our calculations indicate a significant decrease of the heavy-hole effective mass with respect to the bulk GaSb value. However, for some structures under high magnetic fields our calculation predicts a possible enhancement of the heavy-hole effective mass for spin-up states, leading to a large effective mass difference between the heavy-hole up-spin states and the heavy-hole down-spin states. In general, the large variation of the number in Table I reflects the complicated situation of hybridization between different states in different samples under different magnetic field strengths. It is important to mention the difference $m^*_{e,\uparrow}$-$m^*_{e,\downarrow}$ of electronlike effective masses shown in Table I. In cyclotron resonance measurements a similar difference has been observed as a split of the absorption peak.[7] This phenomenon was studied[18] with a six-band model.

In bulk InAs the value of the electron effective g-factor is -15. The values of $g^*_{e,0}$ and $g^*_{e,1}$ for broken-gap quantum wells given in Table II are in general less than this bulk value, except in three cases. In the sample with a 9 nm InAs layer and a 9 nm GaSb layer, large values of $g^*_{e,0}=-17.1$ and $g^*_{e,1}=-18.7$ at the weak magnetic field 1 T are due to the very strong hybridization between electronlike states and light-holelike states. In the same sample, the anticrossing caused by hybridization of electron and heavy-hole states is the origin of the positive $g^*_{e,0}=3.1$ at $B=10$ T. At low magnetic fields, the electron g-factors do not show a monotonic dependence on the interaction strength between the hybridized e-lh levels. The heavy-hole g-factors listed in Table II have a large variation in both magnitude and sign. At $\nu=0$, in all the samples studied here we found negative g-factors at both low and high magnetic fields. At $\nu=1$ the unusually large positive g-factors of the heavy-hole states at high magnetic fields are most likely caused by the interaction with the other states.

TABLE II. Effective g-factors for the highest electronlike states ($g^*_{e,\nu}$) and for the highest heavy-holelike states ($g^*_{hh,\nu}$) in a quantum well with InAs layer width W_{InAs} and GaSb layer width W_{GaSb}, calculated from the energy difference between the $\nu\uparrow$ and the $\nu\downarrow$ states for $\nu=0$ and 1.

(W_{InAs}; W_{GaSb})	B (T)	$g^*_{e,0}$	$g^*_{e,1}$	$g^*_{hh,0}$	$g^*_{hh,1}$
(12 nm; 9nm)	1	−14.305	−14.374	−7.291	−4.682
(12 nm; 9nm)	10	−7.971	−6.314	−2.740	10.437
(12 nm; 9nm)	15	−7.486	−5.867	−0.5747	22.072
(9 nm; 9nm)	1	−17.103	−18.779	−6.738	−4.475
(9 nm; 9nm)	10	3.143	−3.225	−4.805	2.571
(9 nm; 9nm)	15	−5.523	−4.471	−1.099	21.438
(12 nm; 6nm)	1	−8.414	−10.418	−5.356	−2.816
(12 nm; 6nm)	10	−9.761	−6.499	−4.770	6.625
(12 nm; 6 nm)	15	−8.281	−5.895	−2.567	8.420

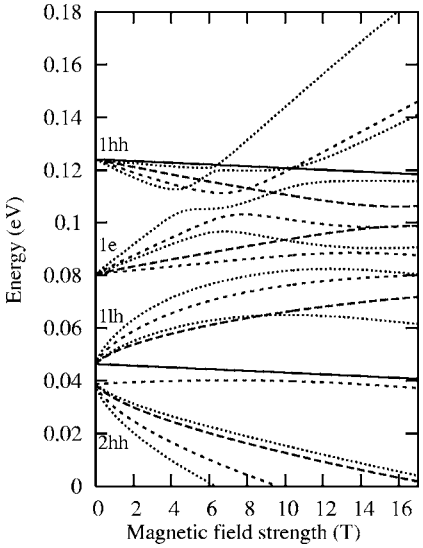

FIG. 8. Similar eigenenergy level structure as in Fig. 5, but calculated non-self-consistently.

V. SELF-CONSISTENT FEATURES

There exist non-self-consistent calculations on the effective g-factor[23] and the cyclotron mass[18] using the six-band model. The relation $|g^*_{e,1}|<|g^*_{e,0}|$ was found as a general feature. In contrast, as shown in Fig. 7, using our self-consistent eight-band model $|g^*_{e,1}|<|g^*_{e,0}|$ holds only in the regime of intermediate magnetic field strength. The electron effective g-factors are usually smaller in the self-consistent eight-band model. The origin of this difference, whether due to the different models and/or the different calculation methods, is an interesting question. The same question applies to the cyclotron effective mass, although the samples used in Ref. 18 are different from ours.

To compare with the non-self-consistent six-band results reported in Ref. 23 we have performed a non-self-consistent eight-band calculation of the Landau level structure in an InAs/GaSb quantum well with a 15 nm InAs layer and a 5 nm GaSb layer. The energy level structures are very similar in the two cases, especially at small magnetic fields. At higher magnetic fields, above ~10 T, however, the Landau levels are slightly different and the anticrossings appear at somewhat higher magnetic field strengths.

Consequently, the difference mentioned above cannot be caused by the different models. Let us instead return to the eight-band model and investigate the InAs/GaSb quantum well with a 12 nm InAs layer and a 6 nm GaSb layer without the effect of charge transfer. The calculated non-self-consistent Landau level structure is shown in Fig. 8, and should be compared with the self-consistent result in Fig. 5. The difference is clear. Relative to the 1hh level, the 1e level is pushed ~20 meV upwards when charge transfer is included. As a consequence, comparing to Fig. 8, the sequence of anticrossings begins at smaller magnetic fields in Fig. 5.

The m^* and g^* of the $0\uparrow$, $0\downarrow$, $1\uparrow$, and $1\downarrow$ electronlike states, corresponding to the non-self-consistent Landau level structure in Fig. 8, are plotted in Fig. 9. Here we see clearly that the shift of anticrossings to higher magnetic fields also moves the abrupt changes of m^* and g^* to higher magnetic fields. While the self-consistent $g^*_{e,1}$ is smooth and $g^*_{e,0}$ is oscillating in Fig. 7, in Fig. 9 the non-self-consistent $g^*_{e,0}$ is smooth but $g^*_{e,1}$ is oscillating. For the effective mass, the non-self-consistent values are larger than the corresponding self-consistent values, and with increasing magnetic field strengths the masses decrease abruptly in Fig. 9 instead of the sharp rising behavior in Fig. 7.

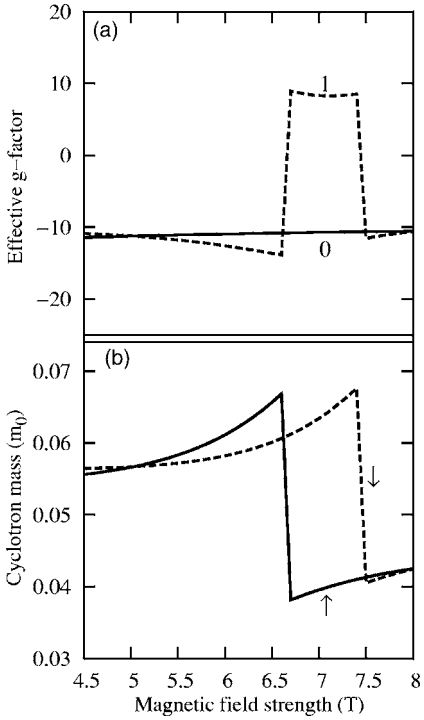

FIG. 9. Effective g-factors $g^*_{e,0}$ and $g^*_{e,1}$ for the non-self-consistent electronlike states in Fig. 8 [panel (a)], and the corresponding cyclotron masses $m^*_{e,\uparrow}$ and $m^*_{e,\downarrow}$ [panel (b)].

VI. COMPARISON WITH EXPERIMENTS

Cyclotron resonance experiments have been performed to measure the effective masses in broken-gap heterostructures. Enhanced electron effective masses and a split of the resonance peak have been observed in different sample structures.[5–8,15] In a study[8] on InAs/GaSb heterostructures, the measured effective mass increases when the InAs layer width is reduced, but decreases when the hybridization is weakened with a spacer. A decreasing value of the effective mass with oscillating behavior was also observed when the applied magnetic field gets stronger.[6] Our calculated results produce qualitatively similar features. The measured electron effective masses vary in the range between $0.035m_0$ and $0.05m_0$, which are smaller than some of our calculated values. This is not surprising because our calculations are performed with samples of a thinner InAs layer and hence hybridization is stronger. As discussed in Sec. V, without the self-consistent potential the calculated mass would be larger. It is important to point out that in our theoretical study we calculate the effective mass of a quasiparticle state with a fixed Landau level index, and investigate how this effective

mass varies with the applied magnetic field strength. In experiments the quasiparticle effective mass is measured at the Fermi level and the observed electron effective mass oscillations occur when the Landau level index of the quasiparticle state at the Fermi level changes. Consequently, our calculated effective mass oscillations are different from those observed experimentally.

In Ref. 7 Marlow *et al.* investigated an InAs/GaSb quantum well with a 15 nm InAs layer and a 10 nm GaSb layer. At a magnetic field $B=5.5$ T and a temperature 3.5 K, the measured effective mass was $0.0345m_0$ and the split of the resonance peak approximately 12 cm^{-1}. We have used a sample with the same thicknesses of the InAs and GaSb layers to perform a calculation at 1.5 K, and obtain $m^*_{e,\uparrow}=0.0356m_0$ and $m^*_{e,\downarrow}=0.0483m_0$. These give a 38 cm^{-1} split of the resonance peak. The discrepancy between the calculated and the measured values is due to a particular difficulty in the self-consistent computation scheme. Namely, it is difficult to tune the self-consistently derived electron and hole densities to the desired values because we do not know the donor concentration, the acceptor concentration, and the type of defects in the experimental samples. The influence of these material parameters on the self-consistent potential is not negligible, especially not in the 15 nm InAs and 10 nm GaSb sample. As a result, our self-consistent electron and hole densities are much higher than those in the experimental samples, leading to a discrepancy between our theoretical self-consistent potential and the actual one in the experimental samples. Consequently, it is unreasonable to expect an accurate quantitative agreement between theoretically calculated and experimentally measured level positions and resonance peak splits.

VII. CONCLUSIONS

We have investigated the influence of hybridization of electron, light-hole, and heavy-hole states on cyclotron masses and g-factors in broken-gap AlSb/InAs/GaSb/AlSb quantum wells under a magnetic field applied perpendicular to the interfaces. In our calculations we used the eight-band $\mathbf{k}\cdot\mathbf{p}$ model and the Burt-Foreman envelope function theory, taking into account the Coulomb interaction between charged carriers as well as the strain induced by lattice mismatch. We can control the hybridization strength by changing the InAs and/or GaSb layer thicknesses, by inserting a thin AlSb barrier between the InAs and GaSb layers, and by varying the magnetic field strength. The electron-light-hole hybridization is increased by making the InAs layer thinner, but decreased by making the GaSb layer thinner. When a barrier is added between the InAs layer and the GaSb layer, the amount of hybridization is reduced if the interaction between electron and light-hole states is relatively weak, but a strong hybridization can also appear if the electron-light-hole interaction is strong.

By changing the thicknesses of various layers in the heterostructure, we have demonstrated the connection between a stronger electron-hole hybridization and a larger electron effective mass. At low and high magnetic fields the hybridization of electrons and light holes enhances the electron effective mass. Along this line of investigation, we have discovered an unusual dependence of the electron cyclotron mass and g-factor on the interaction strength between the electronlike and light-holelike levels. At intermediate magnetic field strengths where the electronlike and the heavy-holelike states anticross, electrons can hybridize strongly with both light and heavy holes. In this region, we found an interesting oscillating behavior of the electron effective masses and g-factors for quasiparticle states with a fixed Landau level index. In addition, the electron g-factor can change sign with increasing magnetic field. Compared to their values in bulk InAs, our calculated electron m^* is enhanced in agreement with previous investigations, while g^* is generally reduced. However, the heavy-hole effective masses are as a rule much smaller than the corresponding values in bulk GaSb, whereas the absolute values of g^* can be unusually large.

APPENDIX

In this Appendix we give the explicit expressions of the operators in our Hamiltonian Eq. (2). The momentum operators and the z-dependent material parameters have been properly ordered. The main difference between our ordering and that in Ref. 30 appears in the matrix elements containing the interband momentum matrix element P. These operators are

$$\hat{A}=\hat{K}_+A_c\hat{K}_-+\hat{K}_-A_c\hat{K}_++\hat{K}_zA_c\hat{K}_z, \tag{A1}$$

$$\hat{D}_\pm=\frac{\hbar^2}{2m_0}\sqrt{2}[2\hat{K}_z\gamma_2\hat{K}_z-\hat{K}_+\gamma_2\hat{K}_--\hat{K}_-\gamma_2\hat{K}_+] \pm\frac{1}{3\sqrt{2}}[\hat{K}_-(N_+-N_-)\hat{K}_+-\hat{K}_+(N_+-N_-)\hat{K}_-], \tag{A2}$$

$$\hat{E}_\pm=-\frac{\hbar^2}{2m_0}[\hat{K}_z\gamma_1\hat{K}_z+\hat{K}_+\gamma_1\hat{K}_-+\hat{K}_-\gamma_1\hat{K}_+] \pm\frac{1}{3}[\hat{K}_-(N_+-N_-)\hat{K}_+-\hat{K}_+(N_+-N_-)\hat{K}_-], \tag{A3}$$

$$\hat{F}_\pm=-\frac{\hbar^2}{2m_0}[\hat{K}_+(\gamma_1+\gamma_2)\hat{K}_-+\hat{K}_-(\gamma_1+\gamma_2)\hat{K}_++\hat{K}_z(\gamma_1-2\gamma_2)\hat{K}_z]\pm\frac{1}{2}[\hat{K}_-(N_+-N_-)\hat{K}_+-\hat{K}_+(N_+-N_-)\hat{K}_-], \tag{A4}$$

$$\hat{G}_\pm=-\frac{\hbar^2}{2m_0}[\hat{K}_z(\gamma_1+2\gamma_2)\hat{K}_z-\hat{K}_+(\gamma_2-\gamma_1)\hat{K}_--\hat{K}_-(\gamma_2-\gamma_1)\hat{K}_+]\pm\frac{1}{6}[\hat{K}_-(N_+-N_-)\hat{K}_+-\hat{K}_+(N_+-N_-)\hat{K}_-], \tag{A5}$$

$$\hat{P}_\pm=-\frac{i}{3}[\hat{K}_z(2N_++N_-)\hat{K}_\pm+\hat{K}_\pm(N_++2N_-)\hat{K}_z], \tag{A6}$$

$$\hat{Q}_{\pm} = \frac{i}{3}[\hat{K}_z(N_+ + 2N_-)\hat{K}_{\pm} + \hat{K}_{\pm}(2N_+ + N_-)\hat{K}_z], \quad \text{(A7)}$$

$$\hat{R}_{\pm} = -\frac{\hbar^2}{2m_0}\sqrt{3}[\hat{K}_+(\gamma_2 \pm \gamma_3)\hat{K}_+ + \hat{K}_-(\gamma_2 \mp \gamma_3)\hat{K}_-], \quad \text{(A8)}$$

$$\hat{S}_{\pm} = -i\sqrt{\frac{2}{3}}[\hat{K}_z N_+ \hat{K}_{\pm} + \hat{K}_{\pm} N_- \hat{K}_z], \quad \text{(A9)}$$

$$\hat{T}_{\pm} = -i\frac{\sqrt{2}}{3}[\hat{K}_z(N_+ - N_-)\hat{K}_{\pm} - \hat{K}_{\pm}(N_+ - N_-)\hat{K}_z], \quad \text{(A10)}$$

where we used the modified Luttinger parameters γ_1, γ_2, and γ_3 to define

$$N_- = -\frac{\hbar^2}{2m_0}(\gamma_1 - 2\gamma_2 + 1) \quad \text{(A11)}$$

and

$$N_+ = -\frac{\hbar^2}{2m_0}(6\gamma_3 - \gamma_1 + 2\gamma_2 - 1). \quad \text{(A12)}$$

The parameter A_c is given by[25]

$$A_c = \frac{\hbar^2}{2m_c} - \frac{2P^2}{3E_g} - \frac{P^2}{3(E_g + \Delta)}, \quad \text{(A13)}$$

where m_c is the conduction band effective mass and E_g the band gap.

The operators in our Hamiltonian can be written in another form with the use of the fourth Luttinger parameter κ. Through the relationship[36] between κ, γ_1, γ_2, and γ_3, κ appears explicitly in $\hat{P}_{\pm}$, $\hat{Q}_{\pm}$, and $\hat{S}_{\pm}$. For example, by defining $\chi = \kappa + 1/3$, we can write $\hat{S}_{\pm}$ as

$$\hat{S}_{\pm} = \frac{\hbar^2}{2m_0} 3i\sqrt{\frac{2}{3}}[\hat{K}_z(\gamma_3 + \chi)\hat{K}_{\pm} + \hat{K}_{\pm}(\gamma_3 - \chi)\hat{K}_z]. \quad \text{(A14)}$$

[1] P. Y. Yu and M. Cardona, *Fundamentals of Semiconductors*, 3rd ed. (Springer, Berlin, 2001).
[2] Y. Guldner, J. P. Vieren, P. Voisin, M. Voos, L. L. Chang, and L. Esaki, Phys. Rev. Lett. **45**, 1719 (1980).
[3] D. Heitmann, M. Ziesmann, and L. L. Chang, Phys. Rev. B **34**, R7463 (1986).
[4] G. M. Sundaram, R. J. Warburton, R. J. Nicholas, G. M. Sammers, N. J. Mason, and P. J. Walker, Semicond. Sci. Technol. **7**, 985 (1992).
[5] Y. Vasilyev, S. Suchalkin, K. von Klitzing, B. Meltser, S. Ivanov, and P. Kop'ev, Phys. Rev. B **60**, 10636 (1999).
[6] J. Kono, B. D. McCombe, J. P. Cheng, I. Lo, W. C. Mitchel, and C. E. Stutz, Phys. Rev. B **55**, 1617 (1997).
[7] T. P. Marlow, L. J. Cooper, D. D. Arnone, N. K. Patel, D. M. Whittaker, E. H. Linfield, D. A. Ritchie, and M. Pepper, Phys. Rev. Lett. **82**, 2362 (1999).
[8] C. Petchsingh, R. J. Nicholas, K. Takashina, N. J. Mason, and J. Zeman, Phys. Rev. B **70**, 155306 (2004).
[9] S. Washburn, R. A. Webb, E. E. Mendez, L. L. Chang, and L. Esaki, Phys. Rev. B **31**, R1198 (1985).
[10] E. E. Mendez, L. Esaki, and L. L. Chang, Phys. Rev. Lett. **55**, 2216 (1985).
[11] J. Luo, H. Munekata, F. F. Fang, and P. J. Stiles, Phys. Rev. B **38**, R10142 (1988).
[12] J. Luo, H. Munekata, F. F. Fang, and P. J. Stiles, Phys. Rev. B **41**, 7685 (1990).
[13] M. J. Yang, C. H. Yang, B. R. Bennett, and B. V. Shanabrook, Phys. Rev. Lett. **78**, 4613 (1997).
[14] M. Lakrimi, S. Khym, R. J. Nicholas, D. M. Symons, F. M. Peeters, N. J. Mason, and P. J. Walker, Phys. Rev. Lett. **79**, 3034 (1997).
[15] K. Suzuki, S. Miyashita, and Y. Hirayama, Phys. Rev. B **67**, 195319 (2003).
[16] M. Altarelli, Phys. Rev. B **28**, 842 (1983).
[17] J. C. Chiang, S. F. Tsay, Z. M. Chau, and I. Lo, Phys. Rev. Lett. **77**, 2053 (1996).
[18] S. F. Tsay, J. C. Chiang, Z. M. Chau, and I. Lo, Phys. Rev. B **56**, 13242 (1997).
[19] G. Grosso, S. Moroni, and G. P. Parravicini, Phys. Rev. B **40**, 12328 (1989).
[20] R. Magri, L. W. Wang, A. Zunger, I. Vurgaftman, and J. R. Meyer, Phys. Rev. B **61**, 10235 (2000).
[21] E. Halvorsen, Y. Galperin, and K. A. Chao, Phys. Rev. B **61**, 16743 (1999).
[22] A. Zakharova, S. T. Yen, and K. A. Chao, Phys. Rev. B **64**, 235332 (2001).
[23] A. Zakharova, S. T. Yen, and K. A. Chao, Phys. Rev. B **69**, 115319 (2004).
[24] M. G. Burt, J. Phys.: Condens. Matter **4**, 6651 (1992).
[25] B. A. Foreman, Phys. Rev. B **56**, R12748 (1997).
[26] I. Lapushkin, A. Zakharova, S. T. Yen, and K. A. Chao, J. Phys.: Condens. Matter **16**, 4677 (2004).
[27] A. Zakharova, I. Lapushkin, S. T. Yen, K. Nilsson, and K. A. Chao, *Recent Research Developments in Science & Technology of Semiconductors* (Transworld Research Network, Kerala, 2004), Vol. 2, p. 37.
[28] A. Zakharova, J. Phys.: Condens. Matter **11**, 4675 (1999).
[29] H. R. Trebin, U. Rössler, and R. Ranvaud, Phys. Rev. B **20**, 686 (1979).
[30] V. Mlinar, M. Tadić, B. Partoens, and F. M. Peeters, Phys. Rev. B **71**, 205305 (2005).
[31] D. Gershoni, C. H. Henry, and G. A. Baraff, IEEE J. Quantum Electron. **29**, 2433 (1993).
[32] G. Y. Wu, T. C. McGill, C. Mailhiot, and D. L. Smith, Phys. Rev. B **39**, 6060 (1989).
[33] K. Nilsson, A. Blom, and V. V. Shlyapin, Solid State Commun. **132**, 178 (2004).
[34] A. Zakharova and K. A. Chao, J. Phys.: Condens. Matter **14**, 5003 (2002).
[35] M. P. C. M. Krijn, Semicond. Sci. Technol. **6**, 27 (1991).
[36] C. R. Pidgeon and R. N. Brown, Phys. Rev. **146**, 575 (1966).